THE JOURNAL OF PHYSICAL CHEMISTRY C

Article

pubs.acs.org/JPCC

Photochemical Hydrogen Production of Ta_2O_5 Nanotubes Decorated with NiO Nanoparticles by Modified Sputtering Deposition

Renato V. Gonçalves,[*,†] Heberton Wender,[‡] Pedro Migowski,[§] Adriano F. Feil,[§] Dario Eberhardt,[§] Jocenir Boita,[∥] Sherdil Khan,[⊥] Giovanna Machado,[&] Jairton Dupont,[%] and Sergio R. Teixeira[*,⊥]

[†]Instituto de Física de São Carlos, Universidade de São Paulo, PO Box 369, 13560-970, São Carlos, SP, Brazil

[‡]Instituto de Física, Universidade Federal do Mato Grosso do Sul (UFMS), Cidade Universitária, CEP 79070-900, Campo Grande, MS, Brazil

[§]PUCRS, Centro Interdisciplinar de Nanociências e Micro-Nanotecnologia (NanoPUC), Av. Ipiranga, 6681, CEP 90619-900, Porto Alegre, RS, Brazil

[∥]Universidade Federal de Santa Maria - UFSM, Campus Cachoeira do Sul, Ernesto Barros, 1345, Santo Antônio, CEP 96506-322, Cachoeira do Sul, RS, Brazil

[⊥]Instituto de Física, Universidade Federal do Rio Grande do Sul (UFRGS), Av. Bento Gonçalves, 9500, Bairro Agronomia, CEP 91501-970, Porto Alegre, RS, Brazil

[&]Centro de Tecnologias Estratégicas do Nordeste − CETENE, Recife, PE, Brazil

[%]School of Chemistry, University of Nottingham, University Park, Nottingham NG7 2RD, U.K.

Supporting Information

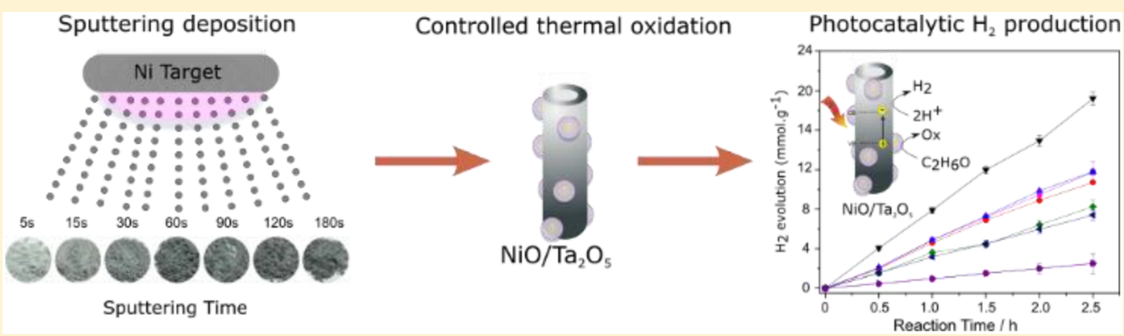

ABSTRACT: The use of metal/oxide nanoparticles (NPs) as cocatalysts in heterogeneous photocatalysis is an important strategy to improve the photocatalytic activity of semiconductors for hydrogen generation. This article reports the use of a modified sputtering deposition method to prepare ultrafine NiO NPs cocatalysts dispersed on anodic Ta_2O_5 nanotubes (NTs). *In situ* X-ray absorption near-edge spectroscopy (XANES) measurements revealed that after exposing the as-prepared Ni NPs to air atmosphere a mixture of 68% of Ni and 32% of NiO was formed. Pure phase NiO NPs was successfully obtained after a controlled thermal oxidation at 500 °C which was confirmed by *in situ* XANES and *ex situ* XPS analyses. The photocatalytic hydrogen production activity was evaluated using ethanol as a sacrificial agent. Ta_2O_5 NTs with 0.16 wt % of NiO showed superior photocatalytic activity (up to 7.7 ± 0.3 mmol h^{-1} g^{-1}) as compared to pure Ta_2O_5 NTs (4.9 ± 0.3 mmol h^{-1} g^{-1}) The observed higher photocatalytic activity suggests that NiO/Ta_2O_5 NTs is a promising material for photocatalytic hydrogen evolution.

1. INTRODUCTION

The total world energy consumption in 2013 was estimated to 13.5 Mtoe (toe = tonne of oil equivalent), value equivalent to an average power consumption of 18.0 terawatts (TW), and the projection for world power consumption in 2050 is around 40.8 TW.[1,2] Moreover, the implementation of policies for diminishing the emission of greenhouse gases in the atmosphere by avoiding the use of fossil fuels is continually increasing.[3] Considering this scenario, hydrogen production by water photolysis is a promising strategy for meeting future energy demands.

The photocatalytic splitting of water using metal oxide semiconductors has been reported as one of the most important strategies for producing hydrogen from water since the Honda−Fujishima report.[4] A number of semiconductor photocatalysts, such as Fe_2O_3,[5] TiO_2,[6] $SrTiO_3$,[7] $KTaO_3$,[8] $NaTaO_3$[9] and Ta_2O_5,[10] have been studied. They show reasonable photolysis efficiency, especially in Ta-based photo-

Received: October 19, 2016
Revised: February 14, 2017
Published: February 27, 2017

DOI: 10.1021/acs.jpcc.6b10540
J. Phys. Chem. C 2017, 121, 5855−5863

catalysts under ultraviolet (UV) light irradiation. Recently, tantalum-based semiconductors have been reported as promising photocatalytic materials with high activity for hydrogen production under ultraviolet or visible light.[10−18] The photocatalytic activity can be improved by loading NiO nanoparticle (NP) cocatalysts onto the surface of these Ta-based materials and has been reported as an important strategy for enhancing the overall activity of photocatalytic water splitting.[19−25]

A variety of routes for synthesizing NiO NP cocatalysts on semiconductor surfaces have been established, including solid-state reaction,[13] impregnation,[26] and sol−gel.[22] However, these methods often lead to the incorporation of counterions and NPs with a broad size distribution. Recently, the magnetron sputtering deposition method has been employed to deposit Pt, Cu, and Ni NPs directly onto the surface of powder catalysts applied to oxidation and hydrogenation reactions and as biocatalysts.[27−30] The main advantage of using the magnetron sputtering method is that it is a clean, controllable, and scalable technique, which can be applied for obtaining an almost limitless NPs composition by properly choosing the sputtering target and the gas composition inside the deposition chamber. Moreover, this method of deposition can be used to produce NPs in liquid or solid substrates, allowing the control of important properties such as NP size,[31,32] shape,[33] and concentration.[34] Thus, the use of the magnetron sputtering method to load NPs onto the surface of powder photocatalysts is a promising strategy for improving their photocatalytic response. However, while sputtering materials over a static powder, one should consider that the top surface of the powders would possess a high concentration of nanoparticles, resulting in a nonuniform material. Therefore, the sputtering process itself presents limitations for a homogeneous distribution of the sputtered NPs over the entire and static powder substrate. The solution to the inhomogeneity of deposited nanoparticles in powder surface is the modification of the conventional sputtering process such that the powder is continuously moved during deposition. Our group has proposed that modification in the form of a resonant mechanical apparatus for agitating the powder substrate at the same time that atoms are ejected from the target during the sputtering process.[27−30]

Herein, we describe the use of this modified magnetron sputtering deposition method to produce uniform NiO cocatalyst NPs on anodic Ta_2O_5 nanotube (NT) powders. The NiO particles were prepared by the controlled thermal oxidation of Ni NPs formed by sputtering bulk Ni targets over the NTs powder. Ni metal oxidation process was studied *in situ* by means of X-ray absorption near-edge structure (XANES) and *ex situ* by X-ray photoelectron spectroscopy (XPS). The photocatalytic activity of the Ta_2O_5 NTs coated with NiO NPs for hydrogen generation was studied.

2. MATERIALS AND METHODS

2.1. General Considerations. All solvents and reagents were of analytical grade and used as received. Tantalum foil (0.25 mm thick, 99.99%) and the nickel-sputtering target (99.99%) were purchased from Goodfellow Corporation. The standard sample of NiO (99.8%) was purchased from Sigma-Aldrich and used as received.

2.2. Synthesis of the Ta_2O_5 NTs. Ta_2O_5 NTs powder was prepared by anodizing tantalum foil in a standard two-electrode electrochemical cell configuration using copper foil as the counter electrode. A constant voltage (50 V) for 20 min was applied between the electrodes immersed in a solution of H_2SO_4 + 1 vol % HF + 4 vol % of deionized water. During anodization, the electrochemical cell was sonicated, and the ultrasonic bath water temperature was maintained at 50 °C using a serpentine coil connected to a heating water bath. The details of this method are described in our previous work.[11] After anodization, the NTs were detached from Ta substrate by sonication in distilled water for 30 min that also helped to separate them from each other and afterward annealed at 800 °C for 60 min.

2.3. Deposition of Ni Nanoparticles. Ni nanoparticles were produced by depositing Ni onto Ta_2O_5 NTs powders (treated at 800 °C for 1 h) using a dc magnetron sputtering deposition system with a specially designed mechanical resonant agitator placed inside the vacuum chamber. The details of the mechanical resonant agitator apparatus have been reported elsewhere.[27−30] Briefly, for sputtering deposition, 100 mg of Ta_2O_5 NTs powder was placed into a glass support connected to the mechanical resonant agitator that permits continuous homogenization of the deposited NPs on the entire powder surface. All sputtering deposition were performed at 150 W under argon working pressure (99.99%, purchased from White Martins-Brazil) fixed at 2×10^{-2} mbar, target-to-agitator distance of 50.0 mm, and sputtering time varying from 5 to 180 s. During deposition, the agitator vibration frequency was maintained at 30 Hz by a sinusoidal wave generation. After deposition process, all samples containing Ni metal were oxidized by calcination at 500 °C in air for 120 min at 10 °C/min.

2.4. Flame Atomic Absorption Spectroscopy (FAAS). The quantification of Ni in the Ta_2O_5 NTs was performed via flame atomic absorption spectroscopy (FAAS) using a Shimadzu AA-6300 apparatus. Initially, 10 mg of NPs/NTs was added to a beaker with 5.0 mL of aqua regia digestive solution and maintained at 110 °C for 3 h. After complete digestion, 5 mL of distilled water was added to the digestive solution, and the product was centrifuged at 7000 rpm for complete separation of the Ta_2O_5 NT support. Prior to analysis, the spectrophotometer was calibrated with standard nickel solutions (0.5, 1.0, and 2.0 ppm), using distilled water as a blank.

2.5. Microscopy Analysis. The morphologies of the Ta_2O_5 NTs and NiO NPs samples were analyzed by field emission scanning electron microscopy (FESEM) using a FEI Inspect F50 (LNLS, proposal no. 13251 e 13057) equipped with an energy dispersive X-ray spectrometer (EDS), and high-resolution transmission electron microscopy (HRTEM) was performed using a JEOL JEM (3010) operated at 300 kV. The samples for HRTEM were prepared by dispersing 1−2 mg of NTs powder in acetone at room temperature followed by sonication. One or two drops were further deposited on a 400 mesh carbon-coated Cu grid.

2.6. Optical Properties. The optical properties of the Ta_2O_5 an NiO/Ta_2O_5 NTs were determined at room temperature by UV−vis diffuse reflectance spectroscopy (UV−Vis Varian Cary 5000) using an integrated sphere accessory and a light wavelength range between 200 and 800 nm. The energy band gaps of the pure Ta_2O_5 and NiO/Ta_2O_5 were determined by extrapolating the linear part of the Tauc plots $(F(R)h\nu)^n$ versus $h\nu$, where R is reflectance, $F(R) = (1 - R)^2/2R$ is the Kubelka−Munk function, and n is determined by the type of transition.

DOI: 10.1021/acs.jpcc.6b10540
J. Phys. Chem. C 2017, 121, 5855−5863

2.7. X-ray Absorption Spectroscopy. To obtain a good XANES signal, a sample with higher Ni concentration was prepared at 20 min of sputtering deposition time. Ni content was confirmed by FAAS with 2.3 wt %. X-ray absorption near-edge structure (XANES) that was performed at the Ni K-edge (8333 eV) in the XAFS1 beamline of the Brazilian Synchrotron Light Laboratory (LNLS) (proposal XAFS1-19024). The sample was heated in a special oven designed for *in situ* XAS experiments from room temperature to 500 °C in air atmosphere. During heat treatment the temperature was increased from 25 to 300 °C with a heating rate of 10 °C min^{-1} and maintained at 300 °C for 120 min, then heated from 300 to 500 °C with a heating rate of 10 °C min^{-1}, and kept at 500 °C for further 120 min. The spectra were collected *in situ* at different temperatures using a channel-cut Si (111) crystal monochromator and three ionization chambers to detect incident and transmitted photon fluxes. Each XANES spectrum was collected about 6 min to obtain enough statistics. To provide good energy reproducibility during data collection, the XANES spectrum of Ni metal foil was simultaneously measured, and the energy was calibrated by aligning the respective absorption edges. Data edge-step normalization was performed after a linear pre-edge subtraction and the regression of a quadratic polynomial beyond the edge, using ATHENA software.[35,36] Standard spectra of NiO and Ni were collected under the same experimental conditions, using sample position for investigation of the presence of NiO in the NPs and further linear combination fittings for all temperature ranges.[36]

2.8. X-ray Photoelectron Spectroscopy. XPS data were collected using a K-Alpha photoelectron spectrometer system (Thermo Scientific) equipped with a monochromatic Al Kα X-ray source (1486.6 eV). During the analysis, the chamber was pumped to ~2×10^{-9} Pa, and the energy steps were 50 and 20 eV for the survey and high-resolution spectra, respectively. The peak fitting was performed using a 70% Gaussian type curve and a 30% Lorentzian type curve and a Tougaard nonlinear sigmoid type baseline. The C 1s peak of adventitious carbon was fixed at 284.8 eV to set the binding energy scale, and the data fitting was performed using CasaXPS software (Casa Software Ltd., UK).

2.9. Photochemical Measurements. Photocatalytic reactions for hydrogen production were carried out in an external irradiation double-wall quartz reactor under continuous magnetic stirring. Samples (8 mg) were dispersed in 8 mL of H_2O:ethanol (4:1 vol) solution and introduced into the reactor. Prior to irradiation, the system was deaerated using Ar−vacuum cycles for about 10 min to reduce the oxygen content. A 300 W xenon lamp (PerkinElmer; Cermax-PE300) was used as light source. During the photocatalytic experiments, the 300 W xenon lamp and the reactor were separated by a fixed distance of 10 cm, and the light source was used with a power of 240 W. The light intensity at the sample was 400 mW cm^{-2} (the intensity of the light source was measured with a Si diode). The temperature during the experiment was maintained at 25 °C using a thermostatic bath. The hydrogen gas produced was quantified by means of a gas chromatograph (Agilent 6820 GC) using a Porapak-Q column 80/100 mesh equipped with a thermal conductivity detector (TCD) connected in series with a methanizer and FID detector. We prepared three identical samples to evaluate reproducibility and quantification the amount of produced gases: H_2, CO, CO_2, CH_4, C_2H_4, and C_2H_6. The measurements were carried out at 0.5 h intervals using a gastight syringe with a maximum volume of 100 μL.

3. RESULTS AND DISCUSSION

3.1. Sputter-Deposited Ni Nanoparticles onto Ta_2O_5 NT Powder. Ta_2O_5 NTs were synthesized by anodization of Ta metal and crystallized at 800 °C for 1 h following the previously optimized conditions for the best photocatalytic activity reported by our group.[11,37] Using a modified sputtering chamber,[27,29,30] different amounts of Ni were deposited on the crystalline Ta_2O_5 NTs powder by varying the sputtering deposition time. The white Ta_2O_5 NTs readily changed to a gray color after 5 s (Figure 1) of sputtering. As the deposition time increased, more Ni NPs were formed on the Ta_2O_5 NTs powder surface, resulting in a darkening of the color. The increase in Ni content was confirmed by FAAS with 0.010, 0.06, 0.16, 0.19, 0.22, 0.26, and 0.47 wt % for the deposition times of 5, 15, 30, 60, 90, 120, and 180 s, respectively.

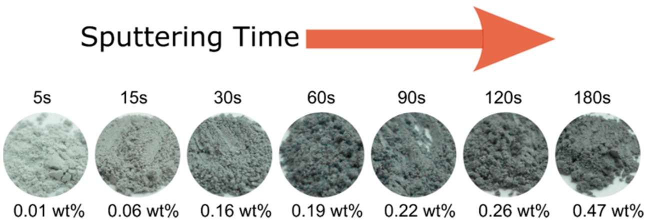

Figure 1. Optical images of Ni NP-loaded Ta_2O_5 NT powders prepared with different sputtering deposition times.

Figure 2a shows the TEM image of Ta_2O_5 NTs decorated with NiO NPs after thermal treatment at 500 °C. It shows that the surface of the Ta_2O_5 NTs was covered with a NiO layer, which was confirmed by energy dispersive X-ray spectroscopy (EDX). The spectrum of the Kα characteristic emission line of Ni around 7.4 keV confirmed the presence of Ni on the Ta_2O_5 NTs surface (inset of Figure 2a). The HRTEM image and corresponding FFT pattern (inset of Figure 2b) reveal the crystalline feature of the Ta_2O_5 NTs. The visible parallel lattice fringes with 0.3098 nm between two adjacent fringes can be assigned to the Ta_2O_5 corresponding to the (200) plane (PDF 25-922). Figure 2b revealed the presence of ultrafine NPs of about 2.0 nm at the external wall of the Ta_2O_5 NTs indicated by blue arrows. Because of the very small size of the NPs the lattice fringes are hardly visible. According to HRTEM image, the sputtering of Ni onto Ta_2O_5 NTs does not alter the original morphology of Ta_2O_5 NTs, as also previously abserved.[11]

3.2. XANES and XPS Study. The oxidation of Ni to NiO is strongly dependent on the calcination parameters, such as temperature and atmosphere, and is usually performed between 300 and 1000 °C in air.[19,26,38] The thermal oxidation of Ni nanoparticles obtained by sputtering to Ni^{2+} in air atmosphere was monitored *in situ* by XANES. The weak X-ray absorption and the high beam attenuation due to the presence of Ta in real samples afforded a poor quality spectrum, and more concentrated ones (2.3 wt % Ni) were needed to provide good quality data in the Ni K-edge region. The linear combination fitting (LCF) of XANES spectra for as-sputtered Ni NPs (starting material for the XAS study) was measured at 25 °C and revealed a mixture of 68% of Ni and 32% of NiO (Figure 3a). It is known that due to their high number of surface atoms, small Ni^0 NPs tend to partially oxidize to Ni^{2+} when stored in air, which explains the presence of the oxide.[39] To investigate the phase transition of Ni^0 to Ni^{2+}, the samples were submitted to thermal treatment up to 500 °C according to

DOI: 10.1021/acs.jpcc.6b10540
J. Phys. Chem. C 2017, 121, 5855−5863

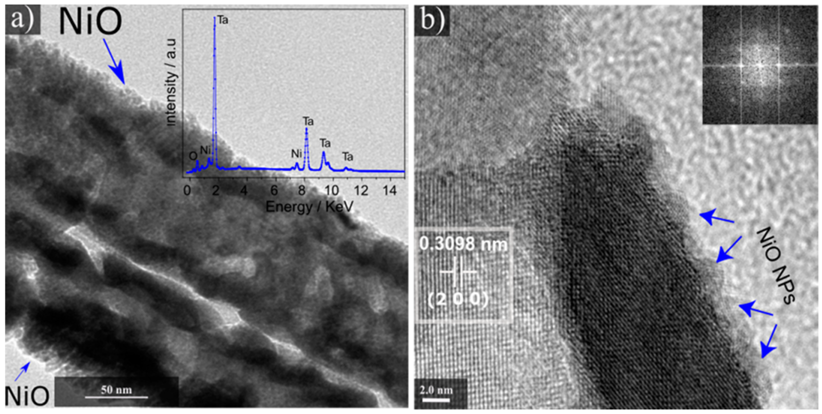

Figure 2. Ta_2O_5 NTs loaded with NiO NPs: (a) TEM and EDS images; (b) HRTEM image and fast Fourier transformation (FFT) patterns of selected area indicated in the figure.

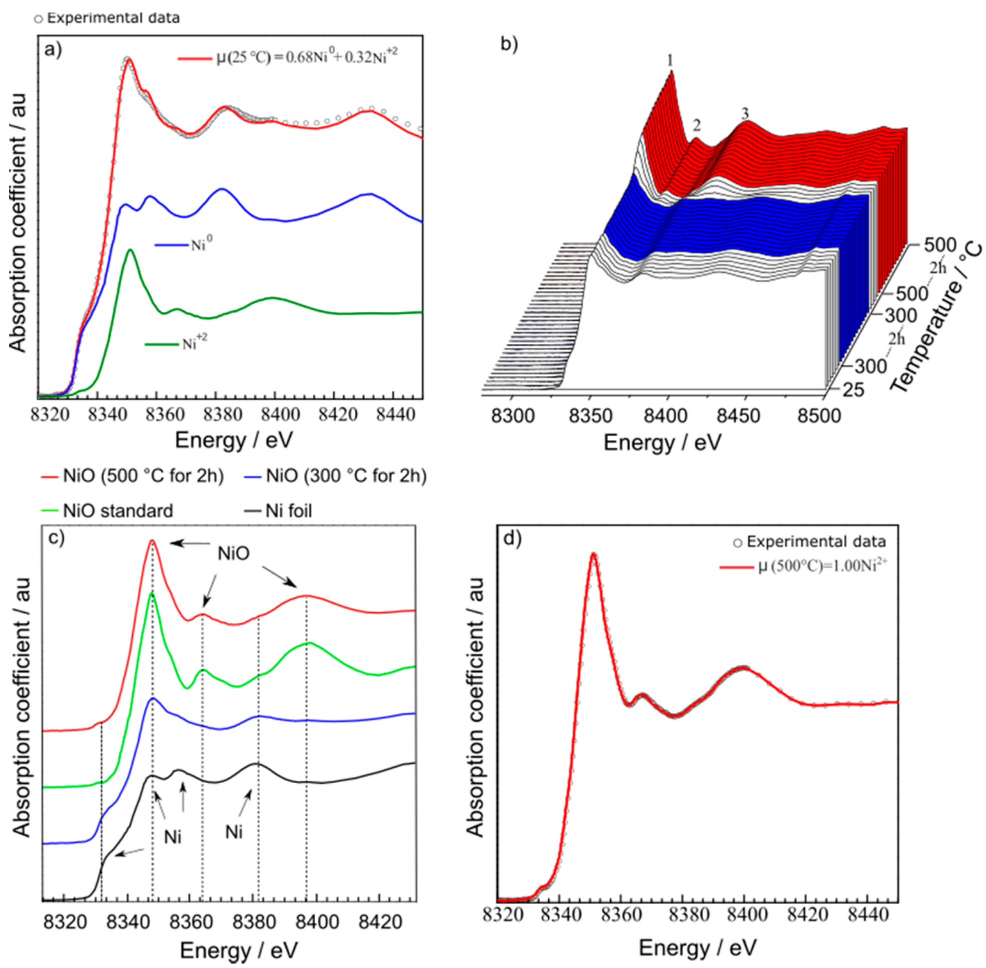

Figure 3. (a) Linear combination fitting for XANES spectrum measured at the Ni K-edge *in situ* at 25 °C (as-prepared sample). (b) *In situ* XANES spectra in room atmosphere for as-prepared NPs catalyst (from room temperature until 500 °C for 2 h). (c) Normalized Ni K-edge XANES spectra for NiO NPs treated at 300 and 500 °C for 2 h, NiO standard, and Ni metal. (d) Linear combination fitting for XANES spectrum measured at the Ni K-edge *in situ* at 500 °C.

the heating ramp described in the Materials and Methods section, and the evolution of XANES spectra as a function of temperature is shown in Figure 3b. The Ni K-edge XANES spectra measured during the thermal treatment until 300 °C showed only slight changes. After treating the sample for 2 h at 300 °C (blue region, Figure 3b) the XANES spectrum has shown a small increase in white line (marked with the number one), indicating the presence of a higher concentration of more localized electronic states characteristic from the decrease of the metallic character of the sample. Increasing the annealing temperature above 300 °C the XANES spectrum presented two new peaks (2 and 3; Figure 3b) at 8365.9 and 8398.6 eV, indicating considerable changes in the composition of the NPs. As the annealing temperature reached 500 °C, peaks 1, 2, and 3

DOI: 10.1021/acs.jpcc.6b10540
J. Phys. Chem. C 2017, 121, 5855−5863

got better defined and pronounced, which can be attributed to oxidation of Ni^0 to NiO (Figure 3b).[40] Maintaining the sample for 2 h at 500 °C (red region, Figure 3b) did not considerably change XANES spectra that indicates all Ni^0 presented in the sample was transformed to NiO. For comparison, Figure 3c shows the normalized XANES spectra at the absorption Ni K-edge for the NiO NPs thermal treated at 300 and 500 °C for 2 h, Ni metal foil, and NiO standards. By a direct comparison, the shoulder near 8334 eV at the Ni K-edge spectra for the sample thermal treated at 300 °C for 2 h resembles the one from Ni foil standard, indicating the presence of Ni^0 in the sample. However, their white line is higher than Ni foil, thereby indicating a mixture oxide/metal phases at 300 °C for 2 h. In fact, the LCF of XANES spectra confirmed a mixture of 65% of NiO and 35% of Ni (Figure S1).

The XANES spectrum of sample thermal treated at 500 °C for 2 h resembles the one from NiO standard and differs completely from that of the standard Ni^0, indicating complete conversion to NiO.[41] The LCF of XANES spectra for sample at 500 °C confirm that the sample has a single phase of NiO (100% of Ni metal was converted until NiO) (Figure 3d).

The surface chemical composition of NiO/Ta_2O_5 NTs was investigated by X-ray photoelectron spectroscopy (XPS). The same sample used in XAS experiments after thermal treatment at 500 °C was analyzed by XPS. The XPS survey spectrum revealed that the sample surface contains Ta, Ni, O, and C (Figure S2). The presence of C 1s on the surface is most probably due to its storage in atmosphere air (C 1s adventitious) and not from sputtering deposition.

The Ni 2p, O 1s, and Ta 4f core-level electrons were investigated to study the chemical and electronic states of nickel and tantalum species in the sample (Figure 4). The XPS spectrum for Ni 2p can be resolved into seven components that can be assigned to NiO nanoparticle surface. Figure 4a showed two low-energy peaks at 855.5 and 853.7 eV corresponding to Ni $2p_{3/2}$ components of Ni^{2+}. The peak at 853.7 eV can be attributed to Ni^{2+}.[42] In the literature, the XPS peak in Ni 2p region at about 855.0 eV has been attributed to the chemical shift of Ni^{3+} species present at the NiO surface.[43] However, the interpretation of the electronic structure of Ni^{2+}/Ni^{3+} has been still a matter of discussion in the literature.[41,43−46] Herein, the Ni 2p curve has two peaks at 855.5 and 853.7 eV which indicates the presence of Ni^{2+}. The fitted satellite peaks at higher energy located at approximately 861 and 865.8 eV have been reported as satellite peaks for stoichiometric NiO.[41] No metallic nickel was detected on the surface of the as-prepared sample by XPS. This result is in good agreement with XANES measurements that showed only a single phase of NiO for the sample thermal treated at 500 °C. Figure 4b shows the Ta 4f region with two asymmetric shape peaks centered at 26.15 and 28.05 eV. These positions fit well with the binding energy of $4f_{7/2}$ and $4f_{5/2}$ components of Ta^{5+} and can be assigned to the Ta_2O_5 phase.[47,48] The O 1s peak in the XPS spectrum of NiO/Ta_2O_5 is shown in Figure 4c where two components centered at 529.4 and 530.6 eV can be identified. The lower binding energy peak located at 529.4 eV and a high binding energy shoulder peak located at 530.6 eV correspond to the NiO and Ta_2O_5, respectively.[48,49] These results confirm that both NiO and Ta_2O_5 are present in the sample.

The optical band gaps of pure Ta_2O_5 and NiO/Ta_2O_5 nanotubes were determined from Tauc plots of diffuse reflectance spectra, as shown in Figure 5.

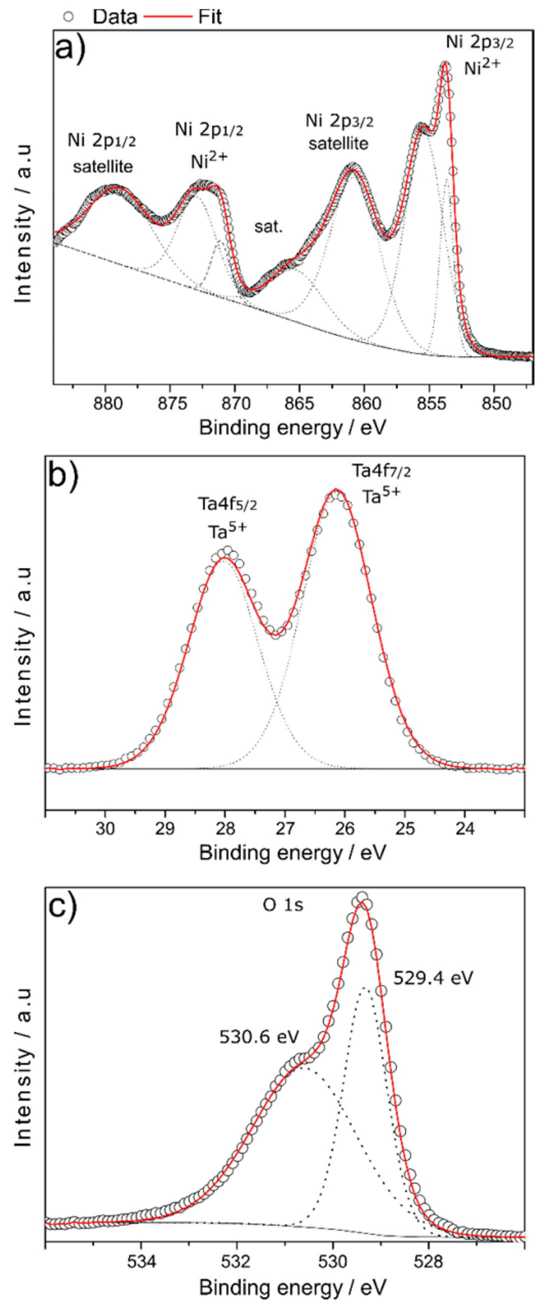

Figure 4. High-resolution XPS spectra for Ni/Ta_2O_5 after thermal treatment at 500 °C for 2 h: (a) Ni 2p, (b) Ta 4f, and (c) O 1s spectrum.

Figure 5 compares the Tauc plots of Ta_2O_5 nanotubes with and without loading NiO nanoparticles. For pure Ta_2O_5 NTs the observed value of the bandgap is 4.45 eV, which is consistent with the reported value in the literature.[10,50] On the other hand, after loading the NiO nanoparticles the bandgap is slightly decreased to 4.41 eV which can be attributed to the combined effect of Ta_2O_5 with NiO having a bandgap of 3.7 eV.

3.3. Photocatalytic Hydrogen Production. Figure 6 displays the hydrogen evolution and the gas composition (H_2, CO, CO_2, C_2H_2, and CH_4) during 2.5 h of reaction time in an H_2O/ethanol solution using pure and NiO loaded Ta_2O_5 NTs. Henceforward, all samples containing NPs were postannealed at 500 °C after sputtering deposition, resulting in a total oxidation of Ni to NiO, as indirectly determined by XANES

DOI: 10.1021/acs.jpcc.6b10540
J. Phys. Chem. C 2017, 121, 5855−5863

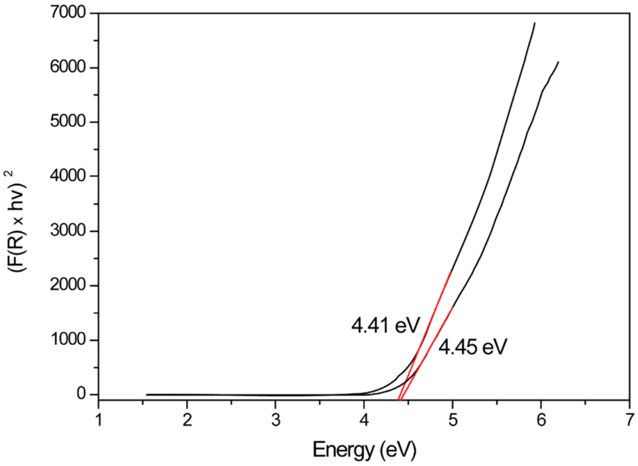

Figure 5. Tauc plot of pure Ta_2O_5 NTs and NiO/Ta_2O_5 NTs with 0.16 wt %.

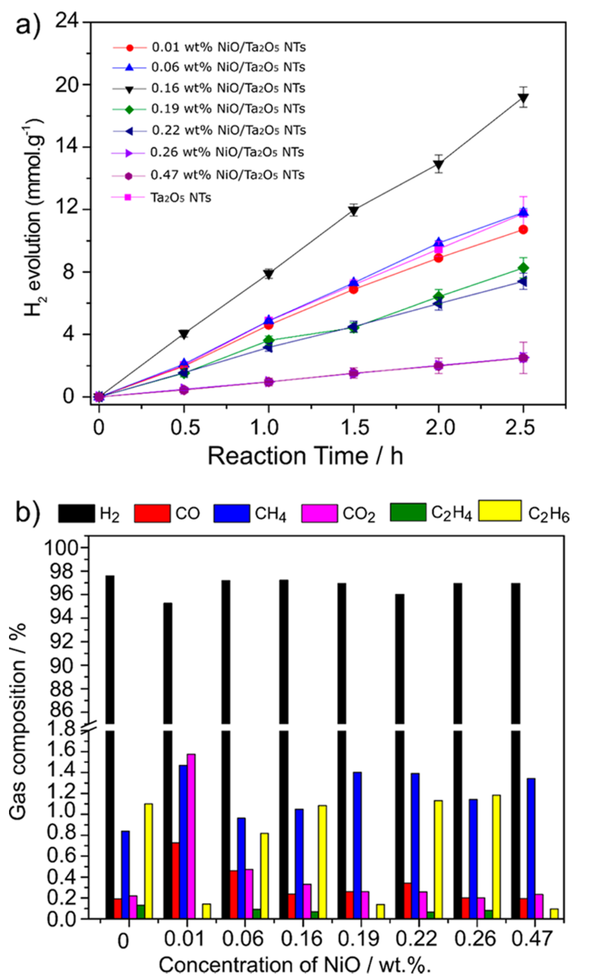

Figure 6. (a) Hydrogen evolution for pure Ta_2O_5 NTs and NTs with different concentrations of NiO NPs on their surface. (b) Products identified in the gas phases after 2.5 h of reaction (rate and yield). Reaction conditions: 20 vol % deaerated aqueous ethanol solution, 8.0 mg of Ta_2O_5 NTs with different loading amounts of NiO NPs.

and XPS. The pure Ta_2O_5 NTs powder produced hydrogen at a rate of 4.9 ± 0.3 mmol h^{-1} g^{-1}.[11] Figure 6a shows that 0.01 and 0.06 wt % NiO/Ta_2O_5 photocatalysts present similar hydrogen evolution activity as pure Ta_2O_5 NTs. When the amount of NiO loaded on the surface of Ta_2O_5 NTs increased to 0.16 wt %, the rate of hydrogen evolution was significantly enhanced to 7.7 ± 0.3 mmol h^{-1} g^{-1}.

The literature has shown that NiO is a p-type semiconductor having light absorption in UV region; on the other hand, Ta_2O_5 presents n-type conductivity. On the basis of the previously reported values for their band positions, we have constructed the energy level diagram (Figure 7) for NiO/Ta_2O_5 hybrid system including the light absorption contribution from NiO.[50,51] The formation of p−n heterojunction will necessitate the electron transfer from NiO to Ta_2O_5 while the hole transfer from Ta_2O_5 to NiO until the system attains carrier diffusion based equilibration between both of the semiconductors. Meanwhile, an inner electric field will be built between NiO and Ta_2O_5 due to that carrier transfer.[52] Upon light irradiation, the available n-type Ta_2O_5 and p-type NiO sites will absorb photon energy higher than or equal to their respective bandgaps; the photogenerated electrons will be excited to their respective conduction bands with simultaneous generation of the holes in the valence bands.[53] Since the conduction band edge of NiO is energetically higher than that of Ta_2O_5, therefore the electrons from the conduction band of NiO will migrate to Ta_2O_5 followed by water reduction. On the other hand, the photogenerated holes from Ta_2O_5 will move to the valence band of NiO followed by ethanol oxidation. Therefore, the presence of NiO NPs in Ta_2O_5 nanotubular matrix contributes to decrease the recombination of the photogenerated carriers in Ta_2O_5 due to the inner electric field at the NiO/Ta_2O_5 interface but also provides an additional light absorption for generating more charge carriers.[53]

One must note that the enhancements in photocatalytic have a strong dependence on the concentration (wt %) of NiO NPs in Ta_2O_5 NTs. Meanwhile, when we increase the sputtering time to increase the concentration of nanoparticles, the Ta_2O_5 sites will be covered with the nanoparticles and the contribution of NiO in the p−n junction will increase and pristine NiO particles are known to present higher recombination centers;[51] therefore, the photocatalytic activity will decrease (Figure 6). Hence, concentration (wt %) of NiO is an important factor that should be sufficient enough to form p−n junction and less enough to not inhibit the light absorbance from Ta_2O_5 NTs. In the current study that concentration has an optimum of 0.16 wt % for the best photocatalytic hydrogen evolution (Figure 6).

The activity of NiO/Ta_2O_5 NTs heterojunction is superior to those reported earlier in the literature under similar conditions, such as tantalum oxide nanotubes (4.9 mmol H_2 g^{-1} h^{-1}),[11] Ta_2O_5 loaded with 5 wt % NiO (0.9 mmol H_2 g^{-1} h^{-1}),[54] $NaTaO_3$:La (2.8 mmol H_2 g^{-1} h^{-1}),[55] and tantalum-based pyrochlore/indium hydroxide nanocomposites (5.8 mmol H_2 g^{-1} h^{-1}).[56] Although slightly more active catalysts have already been reported, they normally need a mixture of doping agents to improve the photoactivity, as observed in the case of La:$NaTaO_3$/NiO[57] or hybrid-like Ta_2O_5/ionic liquid/Pt NPs.[58] However, in our case, the photoactive material is prepared in a simpler and cheaper way than those reported so far.

Figure 6b displays the reaction gas composition after the photocatalytic experiments using Ta_2O_5 NTs with different concentrations of NiO NPs. In addition to H_2 formation during the photocatalytic reaction, other gaseous products were found, namely, carbon monoxide, carbon dioxide, and hydrocarbons such as methane, ethane, and ethylene, and that happened due to the photodecomposition of ethanol.[59,60] However, hydrogen

DOI: 10.1021/acs.jpcc.6b10540
J. Phys. Chem. C 2017, 121, 5855−5863

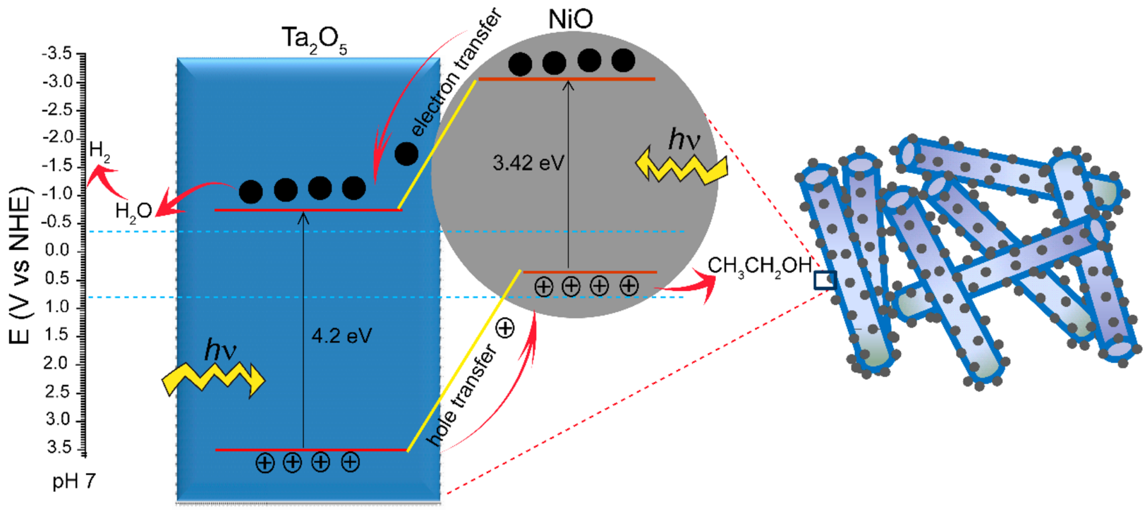

Figure 7. Energy level diagram of NiO NPs/Ta_2O_5 NTs demonstrating the light absorbance and charge transportation of the photogenerated charge carriers for photocatalytic hydrogen production.

was the major product (Figure 6b) for all NiO concentrations, and its concentration was always higher than 95%. The formation of carbon-containing compounds has shown no obvious trend with varying NiO content, and methane and ethane are the major side products formed summing up always ~2% of the gas phase content. The compounds CO and CO_2, originated from organic matter oxidation, are formed in smaller amounts than CH_4 and C_2H_6. Ethylene is formed only in low quantities, with concentrations lower than 0.2%.

4. CONCLUSIONS

In conclusion, the modified magnetron sputtering deposition proved to be a powerful technique for preparing ultrafine NiO NPs cocatalysts dispersed on the surface of Ta_2O_5 NTs powder. The main advantage of using the magnetron sputtering method is that it is a clean, controllable, and scalable technique that can be applied for obtaining NPs of different compositions by properly choosing the sputtering target. The as-sputtered Ni NPs was partially oxidized to 68% of Ni and 32% of NiO after air exposure. The complete oxidation of Ni to NiO NPs was only achieved at 500 °C as could be seen by *in situ* XANES and *ex situ* XPS. Ta_2O_5 NTs loaded with 0.16 wt % of NiO NPs showed the highest photocatalytic activity for hydrogen evolution when compared to pure Ta_2O_5 NTs and other NiO loaded samples. The concentration of p-type NiO is an important feature to hydrogen evolution by photolysis of water that should be sufficient enough to form p-NiO/n-Ta_2O_5 heterojunction and small enough to not inhibit the light absorbance from Ta_2O_5 NTs.

■ ASSOCIATED CONTENT

Supporting Information

The Supporting Information is available free of charge on the ACS Publications website at DOI: 10.1021/acs.jpcc.6b10540.

Linear combination fitting for XANES spectrum measured *in situ* at 300 °C for 2 h (Figure S1); survey XPS spectra for NiO NPs at 500 °C (Figure S2) (PDF)

■ AUTHOR INFORMATION

Corresponding Authors

*(R.V.G.) E-mail: rgoncalves@ifsc.usp.br.

*(S.R.T.) E-mail: durao@if.ufrgs.br.

ORCID

Renato V. Gonçalves: 0000-0002-3372-6647

Jairton Dupont: 0000-0003-3237-0770

Notes

The authors declare no competing financial interest.

■ ACKNOWLEDGMENTS

Our appreciation goes to the following Brazilian funding agencies: CNPq (CNPq-486342/2013-1 and CNPq-471220/2010-8); FAPERGS (FAPERGS-11/2000-4, PqG No. 2235-2551/14-4); and FUNDECT (Process No. 23/200.247/2014). The authors acknowledge LNLS for use of the XAFS1 beamline (XAFS1-19024) and its experimental facilities (INTERCOVAMEX H2 Sputtering System); we also acknowledge LNNano for XPS measurement. Thanks also are due to Prof. Dr Liane M. Rossi for flame atomic absorption spectroscopy measurements.

■ REFERENCES

(1) Lewis, N. S.; Nocera, D. G. Powering the Planet: Chemical Challenges in Solar Energy Utilization. *Proc. Natl. Acad. Sci. U. S. A.* **2006**, *103*, 15729−15735.

(2) *Key World Energy Statistics*; IEA: Paris, 2015; pp 1−77.

(3) Takahashi, T. The Fate of Industrial Carbon Dioxide. *Science* **2004**, *305*, 352−353.

(4) Fujishima, A.; Honda, K. Electrochemical Photolysis of Water at a Semiconductor Electrode. *Nature* **1972**, *238*, 37−38.

(5) Souza, F. L.; Lopes, K. P.; Nascente, P. A. P.; Leite, E. R. Nanostructured Hematite Thin Films Produced by Spin-Coating Deposition Solution: Application in Water Splitting. *Sol. Energy Mater. Sol. Cells* **2009**, *93*, 362−368.

(6) Feil, A. F.; et al. Growth of TiO_2 Nanotube Arrays with Simultaneous Au Nanoparticles Impregnation: Photocatalysts for Hydrogen Production. *J. Braz. Chem. Soc.* **2010**, *21*, 1359−1365.

(7) Kato, H.; Kudo, A. Visible-Light-Response and Photocatalytic Activities of TiO_2 and SrtiO3 Photocatalysts Codoped with Antimony and Chromium. *J. Phys. Chem. B* **2002**, *106*, 5029−5034.

(8) Sun, J.; Chen, G.; Li, Y.; Jin, R.; Wang, Q.; Pei, J. Novel (Na, K)TaO3 Single Crystal Nanocubes: Molten Salt Synthesis, Invariable Energy Level Doping and Excellent Photocatalytic Performance. *Energy Environ. Sci.* **2011**, *4*, 4052.

(9) Kato, H.; Kudo, A. Highly Efficient Decomposition of Pure Water into H2 and O2 over NaTaO3 Photocatalysts. *Catal. Lett.* **1999**, *58*, 153−155.

(10) Zhang, P.; Zhang, J.; Gong, J. Tantalum-Based Semiconductors for Solar Water Splitting. *Chem. Soc. Rev.* **2014**, *43*, 4395−4422.

(11) Gonçalves, R. V.; Migowski, P.; Wender, H.; Eberhardt, D.; Weibel, D. E.; Sonaglio, F. v. C.; Zapata, M. J. M.; Dupont, J.; Feil, A. F.; Teixeira, S. R. Ta2O5 Nanotubes Obtained by Anodization: Effect of Thermal Treatment on the Photocatalytic Activity for Hydrogen Production. *J. Phys. Chem. C* **2012**, *116*, 14022−14030.

(12) Souza, V. S.; Scholten, J. D.; Weibel, D. E.; Eberhardt, D.; Baptista, D. L.; Teixeira, S. R.; Dupont, J. Hybrid Tantalum Oxide Nanoparticles from the Hydrolysis of Imidazolium Tantalate Ionic Liquids: Efficient Catalysts for Hydrogen Generation from Ethanol/Water Solutions. *J. Mater. Chem. A* **2016**, *4*, 7469−7475.

(13) Parida, K. M.; Mahanta, S. K.; Martha, S.; Nashim, A. Fabrication of NiO/Ta2O5 Composite Photocatalyst for Hydrogen Production under Visible Light. *Int. J. Energy Res.* **2013**, *37*, 161−170.

(14) Khan, S.; Zapata, M. J. M.; Baptista, D. L.; Gonçalves, R. V.; Fernandes, J. A.; Dupont, J.; Santos, M. J. L.; Teixeira, S. R. Effect of Oxygen Content on the Photoelectrochemical Activity of Crystallographically Preferred Oriented Porous Ta3N5 Nanotubes. *J. Phys. Chem. C* **2015**, *119*, 19906−19914.

(15) Li, Y.; Takata, T.; Cha, D.; Takanabe, K.; Minegishi, T.; Kubota, J.; Domen, K. Vertically Aligned Ta3N5 Nanorod Arrays for Solar-Driven Photoelectrochemical Water Splitting. *Adv. Mater.* **2013**, *25*, 125−131.

(16) Higashi, M.; Domen, K.; Abe, R. Highly Stable Water Splitting on Oxynitride TaON Photoanode System under Visible Light Irradiation. *J. Am. Chem. Soc.* **2012**, *134*, 6968−6971.

(17) Khan, S.; Zapata, M. J. M.; Pereira, M. B.; Goncalves, R. V.; Strizik, L.; Dupont, J.; Santos, M. J. L.; Teixeira, S. R. Structural, Optical and Photoelectrochemical Characterizations of Monoclinic Ta3N5 Thin Films. *Phys. Chem. Chem. Phys.* **2015**, *17*, 23952−23962.

(18) Zhu, G.; Lin, T.; Cui, H.; Zhao, W.; Zhang, H.; Huang, F. Gray Ta2O5 Nanowires with Greatly Enhanced Photocatalytic Performance. *ACS Appl. Mater. Interfaces* **2016**, *8*, 122−127.

(19) Townsend, T. K.; Browning, N. D.; Osterloh, F. E. Overall Photocatalytic Water Splitting with NiOx-SrTiO3 - a Revised Mechanism. *Energy Environ. Sci.* **2012**, *5*, 9543−9550.

(20) Domen, K.; Kudo, A.; Onishi, T. Mechanism of Photocatalytic Decomposition of Water into H2 and O2 over Nio/SrTiO3. *J. Catal.* **1986**, *102*, 92−98.

(21) Xu, Y.; Xu, R. Nickel-Based Cocatalysts for Photocatalytic Hydrogen Production. *Appl. Surf. Sci.* **2015**, *351*, 779−793.

(22) Sreethawong, T.; Suzuki, Y.; Yoshikawa, S. Photocatalytic Evolution of Hydrogen over Mesoporous Supported Nio Photocatalyst Prepared by Single-Step Sol−Gel Process with Surfactant Template. *Int. J. Hydrogen Energy* **2005**, *30*, 1053−1062.

(23) Liu, Q.; Zhang, L.; Crozier, P. A. Structure−Reactivity Relationships of Ni−NiO Core−Shell Co-Catalysts on Ta2o5 for Solar Hydrogen Production. *Appl. Catal., B* **2015**, *172−173*, 58−64.

(24) Takahara, Y.; Kondo, J. N.; Takata, T.; Lu, D.; Domen, K. Mesoporous Tantalum Oxide. 1. Characterization and Photocatalytic Activity for the Overall Water Decomposition. *Chem. Mater.* **2001**, *13*, 1194−1199.

(25) Sayama, K.; Arakawa, H. Effect of Na2CO3 Addition on Photocatalytic Decomposition of Liquid Water over Various Semiconductor Catalysis. *J. Photochem. Photobiol., A* **1994**, *77*, 243−247.

(26) Husin, H.; Su, W. N.; Chen, H. M.; Pan, C. J.; Chang, S. H.; Rick, J.; Chuang, W. T.; Sheu, H. S.; Hwang, B. J. Photocatalytic Hydrogen Production on Nickel-Loaded LaxNa1-XTaO3 Prepared by Hydrogen Peroxide-Water Based Process. *Green Chem.* **2011**, *13*, 1745−1754.

(27) Gonçalves, R. V.; Wojcieszak, R.; Uberman, P. M.; Eberhardt, D.; Teixeira-Neto, E.; Teixeira, S. R.; Rossi, L. M. Catalytic Abatement of Co over Highly Stable Pt Supported on Ta2O5 Nanotubes. *Catal. Commun.* **2014**, *48*, 50−54.

(28) Luza, L.; Gual, A.; Eberhardt, D.; Teixeira, S. R.; Chiaro, S. S. X.; Dupont, J. "Imprinting" Catalytically Active Pd Nanoparticles onto Ionic-Liquid-Modified Al2O3 Supports. *ChemCatChem* **2013**, *5*, 2471−2478.

(29) Gonçalves, R. V.; Wojcieszak, R.; Wender, H.; Sato B. Dias, C.; Vono, L. L. R.; Eberhardt, D.; Teixeira, S. R.; Rossi, L. M. Easy Access to Metallic Copper Nanoparticles with High Activity and Stability for Co Oxidation. *ACS Appl. Mater. Interfaces* **2015**, *7*, 7987−7994.

(30) Bussamara, R.; Eberhardt, D.; Feil, A. F.; Migowski, P.; Wender, H.; de Moraes, D. P.; Machado, G.; Papaleo, R. M.; Teixeira, S. R.; Dupont, J. Sputtering Deposition of Magnetic Ni Nanoparticles Directly onto an Enzyme Surface: A Novel Method to Obtain a Magnetic Biocatalyst. *Chem. Commun.* **2013**, *49*, 1273−1275.

(31) Wender, H.; de Oliveira, L. F.; Migowski, P.; Feil, A. F.; Lissner, E.; Prechtl, M. H. G.; Teixeira, S. R.; Dupont, J. Ionic Liquid Surface Composition Controls the Size of Gold Nanoparticles Prepared by Sputtering Deposition. *J. Phys. Chem. C* **2010**, *114*, 11764−11768.

(32) Wender, H.; de Oliveira, L. F.; Feil, A. F.; Lissner, E.; Migowski, P.; Meneghetti, M. R.; Teixeira, S. R.; Dupont, J. Synthesis of Gold Nanoparticles in a Biocompatible Fluid from Sputtering Deposition onto Castor Oil. *Chem. Commun.* **2010**, *46*, 7019−7021.

(33) Wender, H.; Goncalves, R. V.; Feil, A. F.; Migowski, P.; Poletto, F. S.; Pohlmann, A. R.; Dupont, J.; Teixeira, S. R. Sputtering onto Liquids: From Thin Films to Nanoparticles. *J. Phys. Chem. C* **2011**, *115*, 16362−16367.

(34) Wender, H.; Migowski, P.; Feil, A. F.; de Oliveira, L. F.; Prechtl, M. H. G.; Leal, R.; Machado, G.; Teixeira, S. R.; Dupont, J. On the Formation of Anisotropic Gold Nanoparticles by Sputtering onto a Nitrile Functionalised Ionic Liquid. *Phys. Chem. Chem. Phys.* **2011**, *13*, 13552−13557.

(35) Newville, M. Ifeffit Interactive XAFS Analysis and Feff Fitting. *J. Synchrotron Radiat.* **2001**, *8*, 322−324.

(36) Ravel, B.; Newville, M. Athena, Artemis, Hephaestus: Data Analysis for X-Ray Absorption Spectroscopy Using Ifeffit. *J. Synchrotron Radiat.* **2005**, *12*, 537−541.

(37) Goncalves, R. V.; Migowski, P.; Wender, H.; Feil, A. F.; Zapata, M. J. M.; Khan, S.; Bernardi, F.; Azevedo, G. M.; Teixeira, S. R. On the Crystallization of Ta2O5 Nanotubes: Structural and Local Atomic Properties Investigated by Exafs and Xrd. *CrystEngComm* **2014**, *16*, 797−804.

(38) Meneses, C. T.; Flores, W. H.; Garcia, F.; Sasaki, J. M. A Simple Route to the Synthesis of High-Quality Nio Nanoparticles. *J. Nanopart. Res.* **2007**, *9*, 501−505.

(39) Karmhag, R.; Niklasson, G. A.; Nygren, M. Oxidation Kinetics of Nickel Nanoparticles. *J. Appl. Phys.* **2001**, *89*, 3012−3017.

(40) Beale, A. M.; Paul, M.; Sankar, G.; Oldman, R. J.; Catlow, C. R. A.; French, S.; Fowles, M. Combined Experimental and Computational Modelling Studies of the Solubility of Nickel in Strontium Titanate. *J. Mater. Chem.* **2009**, *19*, 4391−4400.

(41) Peck, M. A.; Langell, M. A. Comparison of Nanoscaled and Bulk Nio Structural and Environmental Characteristics by Xrd, Xafs, and Xps. *Chem. Mater.* **2012**, *24*, 4483−4490.

(42) Biesinger, M. C.; Payne, B. P.; Lau, L. W. M.; Gerson, A.; Smart, R. S. C. X-Ray Photoelectron Spectroscopic Chemical State Quantification of Mixed Nickel Metal, Oxide and Hydroxide Systems. *Surf. Interface Anal.* **2009**, *41*, 324−332.

(43) Carley, A. F.; Jackson, S. D.; O'Shea, J. N.; Roberts, M. W. The Formation and Characterisation of Ni3+ — an X-Ray Photoelectron Spectroscopic Investigation of Potassium-Doped Ni(110)−O. *Surf. Sci.* **1999**, *440*, L868−L874.

(44) Preda, I.; Mossanek, R. J. O.; Abbate, M.; Alvarez, L.; Méndez, J.; Gutiérrez, A.; Soriano, L. Surface Contributions to the Xps Spectra of Nanostructured Nio Deposited on Hopg. *Surf. Sci.* **2012**, *606*, 1426−1430.

(45) Soriano, L.; Preda, I.; Gutiérrez, A.; Palacín, S.; Abbate, M.; Vollmer, A. Surface Effects in the Ni2p X-Ray Photoemission Spectra of NiO. *Phys. Rev. B: Condens. Matter Mater. Phys.* **2007**, *75*, 233417.

DOI: 10.1021/acs.jpcc.6b10540
J. Phys. Chem. C 2017, 121, 5855−5863

(46) Oku, M.; Tokuda, H.; Hirokawa, K. Final States after Ni2p Photoemission in the Nickel—Oxygen System. *J. Electron Spectrosc. Relat. Phenom.* **1991**, *53*, 201−211.
(47) Goncalves, R. V.; Wojcieszak, R.; Uberman, P. M.; Teixeira, S. R.; Rossi, L. M. Insights into the Active Surface Species Formed on Ta2O5 Nanotubes in the Catalytic Oxidation of Co. *Phys. Chem. Chem. Phys.* **2014**, *16*, 5755−5762.
(48) Atanassova, E.; Spassov, D. X-Ray Photoelectron Spectroscopy of Thermal Thin Ta2o5 Films on Si. *Appl. Surf. Sci.* **1998**, *135*, 71−82.
(49) Wagner, C. D.; Zatko, D. A.; Raymond, R. H. Use of the Oxygen Kll Auger Lines in Identification of Surface Chemical States by Electron Spectroscopy for Chemical Analysis. *Anal. Chem.* **1980**, *52*, 1445−1451.
(50) Chun, W.-J.; Ishikawa, A.; Fujisawa, H.; Takata, T.; Kondo, J. N.; Hara, M.; Kawai, M.; Matsumoto, Y.; Domen, K. Conduction and Valence Band Positions of Ta2O5, TaON, and Ta3N5 by Ups and Electrochemical Methods. *J. Phys. Chem. B* **2003**, *107*, 1798−1803.
(51) Natu, G.; Hasin, P.; Huang, Z.; Ji, Z.; He, M.; Wu, Y. Valence Band-Edge Engineering of Nickel Oxide Nanoparticles Via Cobalt Doping for Application in P-Type Dye-Sensitized Solar Cells. *ACS Appl. Mater. Interfaces* **2012**, *4*, 5922−5929.
(52) Zhang, Z.; Shao, C.; Li, X.; Wang, C.; Zhang, M.; Liu, Y. Electrospun Nanofibers of P-Type Nio/N-Type Zno Heterojunctions with Enhanced Photocatalytic Activity. *ACS Appl. Mater. Interfaces* **2010**, *2*, 2915−2923.
(53) Nail, B. A.; Fields, J. M.; Zhao, J.; Wang, J.; Greaney, M. J.; Brutchey, R. L.; Osterloh, F. E. Nickel Oxide Particles Catalyze Photochemical Hydrogen Evolution from Water—Nanoscaling Promotes P-Type Character and Minority Carrier Extraction. *ACS Nano* **2015**, *9*, 5135−5142.
(54) Sreethawong, T.; Ngamsinlapasathian, S.; Suzuki, Y.; Yoshikawa, S. Nanocrystalline Mesoporous Ta2O5-Based Photocatalysts Prepared by Surfactant-Assisted Templating Sol−Gel Process for Photocatalytic H2 Evolution. *J. Mol. Catal. A: Chem.* **2005**, *235*, 1−11.
(55) Husin, H.; Chen, H. M.; Su, W. N.; Pan, C. J.; Chuang, W. T.; Sheu, H. S.; Hwang, B. J. Green Fabrication of La-Doped Natao3 Via H2o2 Assisted Sol−Gel Route for Photocatalytic Hydrogen Production. *Appl. Catal., B* **2011**, *102*, 343−351.
(56) Hsieh, M. C.; Wu, G. C.; Liu, W. G.; Goddard, W. A., III; Yang, C. M. Nanocomposites of Tantalum-Based Pyrochlore and Indium Hydroxide Showing High and Stable Photocatalytic Activities for Overall Water Splitting and Carbon Dioxide Reduction. *Angew. Chem., Int. Ed.* **2014**, *53*, 14216−20.
(57) Kato, H.; Asakura, K.; Kudo, A. Highly Efficient Water Splitting into H2 and O2 over Lanthanum-Doped NataO3 Photocatalysts with High Crystallinity and Surface Nanostructure. *J. Am. Chem. Soc.* **2003**, *125*, 3082−3089.
(58) Souza, V. S.; Scholten, J. D.; Weibel, D. E.; Eberhardt, D.; Baptista, D. L.; Teixeira, S. R.; Dupont, J. Hybrid Tantalum Oxide Nanoparticles from the Hydrolysis of Imidazolium Tantalate Ionic Liquids: Efficient Catalysts for Hydrogen Generation from Ethanol/Water Solutions. *J. Mater. Chem. A* **2016**, *4*, 7469−7475.
(59) Sakata, T.; Kawai, T. Heterogeneous Photocatalytic Production of Hydrogen and Methane from Ethanol and Water. *Chem. Phys. Lett.* **1981**, *80*, 341−344.
(60) Murdoch, M.; Waterhouse, G. I. N.; Nadeem, M. A.; Metson, J. B.; Keane, M. A.; Howe, R. F.; Lorca, J.; Idriss, H. The Effect of Gold Loading and Particle Size on Photocatalytic Hydrogen Production from Ethanol over Au/TiO_2 Nanoparticles. *Nat. Chem.* **2011**, *3*, 489−492.

DOI: 10.1021/acs.jpcc.6b10540
J. Phys. Chem. C 2017, 121, 5855−5863